Received March 2004
Revised June 2005
Accepted September 2005

An FE-based sequential inverse algorithm for heat flux calculation during impingement water cooling

Mohamed S. Gadala and Fuchang Xu
Department of Mechanical Engineering, University of British Columbia, Vancouver, Canada

Abstract

Purpose – To develop an effective and reliable procedure for the calculation of heat fluxes from the measured temperatures in experimental tests of impingement water cooling.

Design/methodology/approach – An inverse heat transfer analysis procedure is developed and implemented into a 2D finite element program. In this method, the least-squares technique, sequential function specification and regularization are used. Simplifications in the sensitivity matrix calculation and iterative procedures are introduced. The triangular and impulse-like profiles of heat fluxes simulating practical conditions of impingement water cooling are used to investigate the accuracy and stability of the proposed inverse procedure. The developed program is then used to determine the heat flux during impingement water cooling.

Findings – A hybrid procedure is developed in which inverse calculations are conducted with a computation window. This procedure may be used as a whole time domain method or become a periodically sequential or real sequential method by adjusting the sequential steps.

Originality/value – Parametric study and application show that the developed method is effective and reliable and that inverse analysis may obtain the heat flux with an acceptable level of accuracy.

Keywords Heat conduction, Water, Cooling systems, Finite element analysis

Paper type Research paper

Introduction

An inverse heat conduction problem (IHCP) means that the boundary conditions (BC) or material properties are not fully specified, and that they are determined from the measured internal temperature profiles. Because the effects of changes in BC are usually lagged and damped; i.e. the varying magnitude of the interior temperature profile lags behind the changes in BC and is generally of lesser magnitude, an IHCP would be a typically ill-posed problem and would normally be sensitive to the measurement errors. In general, the uniqueness and stability of an IHCP solution are not guaranteed (Beck *et al.*, 1985; Weber, 1981; Alifanov, 1994).

A variety of numerical methods and computational algorithms have been developed to obtain a reliable heat transfer inverse solution. Among these are the least-square regularization method (Beck *et al.*, 1985, 1996), the sequential function specification method (Beck *et al.*, 1996; Kim, 2001), the space marching technique (Weber, 1981), the conjugate gradient method (Alifanov, 1994; Khache and Jarny, 2001), and the maximum entropy method (Kim and Lee, 2002). Important applications of these methods and their numerous modifications have been performed in various branches of thermal engineering such as quenching and hot rolling as well as controlled cooling of steel (Bass, 1980; Beck *et al.*, 1996; Liu *et al.*, 2002; Osman, 1990; Videcoq and Petit, 2001).

International Journal of Numerical Methods for Heat & Fluid Flow
Vol. 16 No. 3, 2006
pp. 356-385

0961-5539
DOI 10.1108/09615530610649762

The determination of the surface heat flux or the surface heat transfer coefficient (HTC) is an important issue among the objectives of the IHCP and, therefore, it has been extensively studied. Improvements and adaptations of the numerical algorithms to complex applications, such as water cooling of hot plates by jet impingement on run-out tables, are still an active area of research for obtaining stable and reliable results.

In this paper, the least-squares method, sequential function specification, regularization, and iterative technique are used and are implemented into a two-dimensional finite element (2D FE) program for analysing IHCP to obtain a higher accuracy and reliability of the inversely calculated heat flux and surface temperature.

Parametric studies have been performed with abrupt heat flux inputs simulating those that occur in run-out table applications. In this treatment, directly calculated internal temperatures under the specially designed heat flux inputs are assigned with artificial random errors and are assumed to be the virtually measured input temperatures. The effects of different values of the number of future time steps and the regularization parameters are numerically investigated, and general guidelines for the application of the algorithm to practical cases are developed.

The inverse analysis algorithm is then applied to obtain the heat flux on the top surface from internal thermocouple measurements of temperature at points beneath the surface at a small distance of about 1 mm. Calculation results of the heat flux values and boiling curves are compared with those available in literatures.

Formulation for direct analysis

The modelling and experimental procedures are based on a 2D planar and axisymmetric assumption. For completeness of the treatment, a brief outline of the equations for direct FE formulation of the transient conduction heat transfer problem is given in the following section. A detailed account of this formulation and equations may be found in reference, Bathe (1982).

The general governing equation for 2D conduction heat transfer problems, shown in Figure 1, is written in the form:

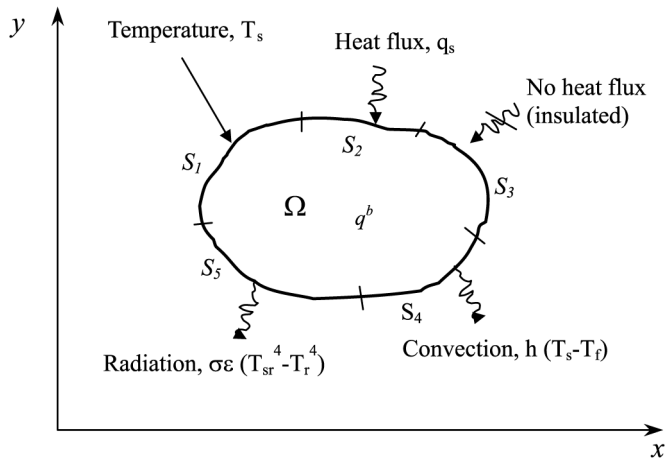

Figure 1.
Boundary conditions for a general conduction problem

$$\frac{\partial}{\partial x}\left(k_x\frac{\partial T}{\partial x}\right)+\frac{\partial}{\partial y}\left(k_y\frac{\partial T}{\partial y}\right)+q^b=c_p\rho\frac{\partial T}{\partial t} \tag{1}$$

where T is the temperature, °C; q^b is the heat generation per unit volume, W/m^3; k_x and k_y are the conductivities in the x- and y-directions, respectively, W/m°C; ρ is the density, kg/m^3; c_p is the specific heat, J/kg°C; t is the time, s; and x, y are the Lagrangian coordinates of the point.

All kinds of the BC such as prescribed temperature, heat flux and convection and radiation as well as their combinations have been implemented in our program. Only the prescribed heat flux is presented here and the others can be found in Appendix.

The specified heat flux ($\mathbf{q}_s$) may be a spatial and/or time function:

$$-\left(k_x\frac{\partial T}{\partial x}+k_y\frac{\partial T}{\partial y}\right)=\mathbf{q}_s(x,y,t)\ \text{ on }\ S_2 \tag{1a}$$

where $\mathbf{q}_s$ is the specified heat flow per unit area in W/m^2. Prescribed heat flux is an example of Cauchy's or Neumann's BC. If $\mathbf{q}_s$ is zero, it will represent a natural BC.

With the use of a weighted residual Galerkin procedure, the final finite element equations may be written as:

$$\mathbf{C}\dot{\mathbf{T}}+\mathbf{K}\mathbf{T}=\mathbf{Q} \tag{2}$$

where $\mathbf{C}$ is the equivalent heat capacity matrix; $\mathbf{K}$ is the equivalent heat conduction matrix; $\mathbf{T}$ and $\dot{\mathbf{T}}$ are vectors of the nodal temperature and its derivatives, respectively; $\mathbf{Q}$ is the equivalent load vector. Detailed expressions of the matrices in equation (2) are given in Appendix.

A general family of solution algorithms for equation (2) may be obtained by introducing a parameter α where ($0.0 \le \alpha \le 1.0$) such that:

$${}^{t+\alpha\Delta t}\dot{\mathbf{T}}=\frac{1}{\Delta t}({}^{t+\Delta t}\mathbf{T}-{}^{t}\mathbf{T})=\frac{1}{\alpha\Delta t}({}^{t+\alpha\Delta t}\mathbf{T}-{}^{t}\mathbf{T}) \tag{3}$$

$${}^{t+\alpha\Delta t}\mathbf{T}=\alpha\,{}^{t+\Delta t}\mathbf{T}+(1-\alpha)\,{}^{t}\mathbf{T} \tag{4}$$

If $\alpha = 0$, an explicit Euler forward method is obtained; if $\alpha = 1/2$, an implicit trapezoidal rule is obtained; and if $\alpha = 1$, an implicit Euler backward method is obtained.

Substituting equation (3) into equation (2) and applying Newton-Raphson iterations yields:

$$\begin{aligned}&{}^{t+\alpha\Delta t}\left[\mathbf{K}+\left(\frac{1}{\alpha\Delta t}\right)\mathbf{C}\right]^{(i-1)}\Delta\mathbf{T}^{(i)}\\&={}^{t+\alpha\Delta t}(\mathbf{Q}^b+\mathbf{Q}^s)+{}^{t+\alpha\Delta t}(\hat{\mathbf{Q}}^h+\hat{\mathbf{Q}}^r)^{(i-1)}-{}^{t+\alpha\Delta t}(\hat{\mathbf{Q}}^c+\hat{\mathbf{q}}^c)^{(i-1)}\end{aligned} \tag{5}$$

where $\alpha \neq 0$. The definitions of all terms are given in Appendix and all quantities at time ($t + \alpha\Delta t$) are calculated from a relation similar to equation (4).

Depending on the value of α, the procedure may be either conditionally stable ($\alpha < 0.5$) or unconditionally stable $\alpha \ge 0.5$.

In the developed program, the geometry domain can be discretized into an assembly of triangular and quadrilateral isoparametric finite elements. The triangular

elements may have three or six nodes while the quadrilateral elements may have four, eight, or nine nodes.

Nonlinearities may arise from the dependence of thermophysical properties on temperature, as in the case of a radiation boundary condition. In the developed program, nonlinearities are handled in a step-wise staggered approach; i.e. the values of the parameters at the current step are calculated based on the temperature at the previous step and are assumed to be constant during the current step. The heat generation due to phase transformation is treated in a similar way.

Formulation for inverse analysis

The IHCP may be generally converted into an optimisation problem. The objective function of the optimisation problem may be considered as the sum of the squares of the differences between the calculated and measured temperatures. To reduce the sensitivity of the IHCP solution to measurement errors and improve the simulation, the data at a number of future time steps (n_{FTS}) are employed in the analysis of the current step. This means that in addition to the measured temperature at the current time step T^i, the measured temperatures at future time steps $T^{i+1}, T^{i+2}, \ldots, T^{i+n_{\mathrm{FTS}}}$ are also used to estimate the heat flux $\mathbf{q}^i$.

A temporary assumption, normally called function specification, would normally be considered for the values of $\mathbf{q}^{i+1}, \mathbf{q}^{i+2}, \ldots, \mathbf{q}^{i+n_{\mathrm{FTS}}}$. The function specification technique works as a regularization procedure that stabilizes the solution process.

To damp the fluctuation of the solution due to measurement errors, the objective function may be made more extensive by including more terms in the expression. A commonly used variable in this regard is a scalar quantity based on the heat flux vector $\mathbf{q}$. This scalar term may be employed with a weighting factor α that is normally called the regularization parameter. Higher order regularization terms involving spatial derivates of $\mathbf{q}$ are not normally adopted.

Based on the above discussion, an objective function in the least-squares method, with future time steps techniques and regularization, may be expressed as follows:

$$F(\mathbf{q}) = \sum_{i=1}^{N} \left(\mathbf{T}_{\mathrm{m}}^i - \mathbf{T}_{\mathrm{c}}^i\right)^{\mathrm{T}} \left(\mathbf{T}_{\mathrm{m}}^i - \mathbf{T}_{\mathrm{c}}^i\right) + \alpha \sum_{i=1}^{N} \mathbf{q}^{i\mathrm{T}} \mathbf{q}^i \tag{6}$$

where $\mathbf{T}_{\mathrm{m}}^i, \mathbf{T}_{\mathrm{c}}^i$ are the experimentally measured and the theoretically calculated temperature vectors at the ith time step in a computation window of size N, respectively; $\mathbf{q}^i$ is the heat flux vector at the ith time step, α is the regularization parameter, and N is the number of total steps considered in the computation window.

The heat flux and temperature vectors are:

$$\mathbf{q} = [\, \mathbf{q}^1 \quad \mathbf{q}^2 \quad \cdots \quad \mathbf{q}^N \,]^{\mathrm{T}} \tag{7a}$$

$$\mathbf{q}^i = [\, \mathbf{q}_1^i \quad \mathbf{q}_2^i \quad \cdots \quad \mathbf{q}_J^i \,]^{\mathrm{T}} \tag{7b}$$

$$\mathbf{T}_{\mathrm{m}}^i = [\, \mathbf{T}_{1\mathrm{m}}^i \quad \mathbf{T}_{2\mathrm{m}}^i \quad \cdots \quad \mathbf{T}_{L\mathrm{m}}^i \,]^{\mathrm{T}} \tag{8}$$

$$\mathbf{T}_{\mathrm{c}}^i = [\, \mathbf{T}_{1\mathrm{c}}^i \quad \mathbf{T}_{2\mathrm{c}}^i \quad \cdots \quad \mathbf{T}_{L\mathrm{c}}^i \,]^{\mathrm{T}} \tag{9}$$

where L is the number of measurement points, and J is the number of heat flux components that can be determined for the flux space distribution on the surface. It should be noted that J must be less than or equal to L. It should also be noted that the dimensions of the heat flux vector $\mathbf{q}^i$ at each step is $1 \times J$, while the total heat flux vector $\mathbf{q}$ is $J \times N$ as it includes the data in N steps; and the temperature vector $\mathbf{T}^i$ at each step is $1 \times L$.

Equation (6) may be written as:

$$F(\mathbf{q}) = \sum_{i=1}^{N} \left(\mathbf{T}_{\mathrm{m}}^i - \mathbf{T}_{\mathrm{c}}^i\right)^{\mathrm{T}} \left(\mathbf{T}_{\mathrm{m}}^i - \mathbf{T}_{\mathrm{c}}^i\right) + \alpha \mathbf{q}^{\mathrm{T}} \mathbf{q} \tag{10}$$

It should be noted that the temperature $\mathbf{T}^k$ would be determined or affected only by the heat fluxes $\mathbf{q}^m$ where $m \leq k$. Mathematically, we may express $\mathbf{T}^k$ as an implicit function of the heat flux:

$$\mathbf{T}_{\mathrm{c}}^k = f(\mathbf{q}^1, \mathbf{q}^2, \ldots, \mathbf{q}^k) \tag{11a}$$

or in a successive form as:

$$\begin{aligned} \mathbf{T}_{\mathrm{c}}^k &= f\left(\mathbf{T}_{\mathrm{c}}^{k-1}, \mathbf{q}^k\right) \\ \mathbf{T}_{\mathrm{c}}^{k-1} &= f\left(\mathbf{T}_{\mathrm{c}}^{k-2}, \mathbf{q}^{k-1}\right) \\ &\vdots \\ \mathbf{T}_{\mathrm{c}}^2 &= f\left(\mathbf{T}_{\mathrm{c}}^1, \mathbf{q}^2\right) \\ \mathbf{T}_{\mathrm{c}}^1 &= f\left(\mathbf{T}_{\mathrm{c}}^0, \mathbf{q}^1\right) \end{aligned} \tag{11b}$$

As a result, the following equation can be obtained:

$$\mathbf{T}_{\mathrm{c}}^k = \mathbf{T}_{\mathrm{c}}^{k^*} + \frac{\partial \mathbf{T}_{\mathrm{c}}^1}{\partial \mathbf{q}^1}(\mathbf{q}^1 - \mathbf{q}^{1^*}) + \frac{\partial \mathbf{T}_{\mathrm{c}}^2}{\partial \mathbf{q}^2}(\mathbf{q}^2 - \mathbf{q}^{2^*}) + \cdots + \frac{\partial \mathbf{T}_{\mathrm{c}}^k}{\partial \mathbf{q}^k}(\mathbf{q}^k - \mathbf{q}^{k^*}) \tag{12}$$

The values with an "*" superscript in equation (12) may be considered as initial guess values that would ultimately lead the temperature $\mathbf{T}_{\mathrm{c}}^{k^*}$.

Here we define the first derivative of temperature $\mathbf{T}_{\mathrm{c}}^i$ with respect to heat flux $\mathbf{q}^i$ as the sensitivity matrix:

$$\mathbf{X}^i = \frac{\partial \mathbf{T}_{\mathrm{c}}^i}{\partial \mathbf{q}^i} = \begin{bmatrix} a_{11}(i) & a_{12}(i) & \cdots & a_{1J}(i) \\ a_{21}(i) & a_{22}(i) & \cdots & a_{2J}(i) \\ \vdots & \vdots & \ddots & \vdots \\ a_{L1}(i) & a_{L2}(i) & \cdots & a_{LJ}(i) \end{bmatrix} \tag{13}$$

$$a_{rs}(i) = \frac{\partial T^i_{cr}}{\partial q^i_s}$$

where $i = 1, 2, \ldots, N$, $r = 1, 2, \ldots, L$, and $s = 1, 2, \ldots, J$. The sensitivity matrix $\mathbf{X}^i$ is an $L \times J$ matrix.

The optimality of the objective function may be obtained by letting $\partial F/\partial \mathbf{q} = 0$ (note that $\partial F/\partial \mathbf{q}$ should be done with respect to each component $\mathbf{q}^i$, with $i = 1, 2, \ldots, N$), and as a result we get the following set of equations:

$$\left\{ \sum_{i=1}^{N} \left(\frac{\partial \mathbf{T}^i_c}{\partial \mathbf{q}^j} \right)^T_{\mathbf{q}^j = \mathbf{q}^{j*}} \left(\frac{\partial \mathbf{T}^i_c}{\partial \mathbf{q}^j} \right)_{\mathbf{q}^j = \mathbf{q}^{j*}} + \alpha \mathbf{I} \right\} (\mathbf{q}^j - \mathbf{q}^{j*}) = \sum_{i=1}^{N} \left(\frac{\partial \mathbf{T}^i_c}{\partial \mathbf{q}^j} \right)^T_{\mathbf{q}^j = \mathbf{q}^{j*}} \left(\mathbf{T}^i_m - \mathbf{T}^{i*}_c \right) - \alpha \mathbf{q}^{j*} \quad j = 1, 2, \ldots, N \tag{14}$$

where $\mathbf{q}^{j*}$ is the initial guess of heat fluxes, and $\mathbf{T}^{i*}_c$ is the calculated temperature vector with the initial guess values.

Recalling equations (12)-(14) may be rearranged and rewritten in the following form:

$$\left(\mathbf{X}^T_{\mathbf{q}=\mathbf{q}^*} \mathbf{X}_{\mathbf{q}=\mathbf{q}^*} + \alpha \mathbf{I} \right) (\mathbf{q} - \mathbf{q}^*) = \mathbf{X}^{\mathrm{T}} \Delta \mathbf{T} - \alpha \mathbf{q}^* \tag{15}$$

where $\mathbf{X}$ is labeled as the total sensitivity matrix for a multi-dimensional problem and has the following form:

$$\mathbf{X} = \begin{bmatrix} \mathbf{X}^1 & 0 & 0 & 0 \\ \mathbf{X}^2 & \mathbf{X}^1 & 0 & 0 \\ \vdots & \vdots & \ddots & 0 \\ \mathbf{X}^N & \cdots & \mathbf{X}^2 & \mathbf{X}^1 \end{bmatrix} \tag{16a}$$

and:

$$\Delta \mathbf{T} = \begin{pmatrix} \mathbf{T}^1_m - \mathbf{T}^{1*}_c & \mathbf{T}^2_m - \mathbf{T}^{2*}_c & \cdots & \mathbf{T}^N_m - \mathbf{T}^{N*}_c \end{pmatrix}^{\mathrm{T}} \tag{17}$$

It should be noted that the dimension of matrix $\mathbf{X}$ is $(L \times N) \times (J \times N)$ and $\Delta \mathbf{T}$ has dimensions of $(L \times N)$. Also, it is worth noting that performing the calculation in equation (15) may be easily done in the time domain, and no function specification for $\mathbf{q}^i$ is needed. If the total sensitivity is known, no iteration is required to get a final solution.

Iterative and sequential algorithms

The form of the governing differential equation for both the temperature $\mathbf{T}(\mathbf{x}, t)$ and the sensitivity coefficient $\mathbf{X}$ $(\mathbf{x}, t)$ is same (Beck *et al.*, 1985) and, therefore, the same finite element program may be used to calculate them. While this is efficient from the

programming point of view, it may not be practical, especially when the temperature time history is somewhat long, the density of mesh is high, and the coefficients at all points are not all needed to get the heat flux $\mathbf{q}$.

An alternative way is to calculate the sensitivity matrices at each time step for the target points. Such a procedure would still require an extensive calculation time and a higher cost when the number of time steps considered and/or the number of heat flux components are reasonably large.

A perturbation algorithm (Liu *et al.*, 2002) was used to obtain the sensitivity matrices $\mathbf{X}^1$ (only the information at the current step was included in the work presented in Liu *et al.* (2002)). First, a given value $\mathbf{q}^{1^*}$ is assumed for all components of the heat flux vector $\mathbf{q}^1$; the direct heat transfer calculation is conducted to get the temperature distribution, say $\mathbf{T}_0^1$, for the given future steps at each thermocouple location. Then, one component of heat flux $\mathbf{q}^1$, say the *J*th component, is increased a reasonable amount, such as 10 per cent, to obtain new temperatures, $\mathbf{T}_J^1$. The ratios of temperature difference at each thermocouple location to the difference of *J*th heat flux component are the sensitivity coefficients. Such a perturbation is repeated for each component of the heat flux $\mathbf{q}^{1^*}$ until all sensitivity matrix components of $\mathbf{X}^1$ are obtained.

The above method would be adopted in this study. By applying this approach, several issues should be resolved. First, the heat fluxes $\mathbf{q}^{i^*}$ for $i = 2, \ldots, N$ in the consecutive steps should be assigned. As mentioned, the function specification would stabilize the solution process. Moreover, it would simplify the calculation of the total sensitivity matrix $\mathbf{X}$. We hereby use a constant assumption, i.e. $\mathbf{q}^{1+k^*} = \mathbf{q}^{1^*} = \mathbf{q}^*$ for $1 \le k \le n_{\mathrm{FTS}}$. Therefore, all sensitivity matrices $\mathbf{X}^i$ for $i = 1, 2, \ldots, N$ may be obtained from the above method by one assignment when the direct calculation is performed for N steps.

The second issue is nonlinearity. The whole sensitivity matrix $\mathbf{X}$ is independent of the heat flux $\mathbf{q}$ only if the conductivity k and specific heat c_p are not functions of the temperature or if the average values for these quantities are used when the dependencies on temperature exist. The thermophysical properties of most steels are temperature dependent. If this kind of dependency is considered, all properties should be updated at the beginning of each time step, which is time-consuming, especially for large size models. Moreover, such changes in properties would not be very large and would not significantly change the magnitude of $\mathbf{X}$. Also, updating the material properties at the beginning of each time step would be based on the temperatures $\mathbf{T}^{k^*}$ obtained from the initially given values of heat flux $\mathbf{q}^*$, which is essentially an approximation. The assumption of a constant value is, therefore, justified. As a slight modification to the above assumption, we may choose to update the sensitivity matrix $\mathbf{X}$ every M steps (in our numerical experiments, $M = 10$). Both methods led to similar results of inverse calculation, so the use of constant sensitivity matrix is justified.

Other factors affecting the accuracy of the calculated heat fluxes are the future information and the addition of regularization parameters. To improve the accuracy due to these factors, the iterative technique with convergence limits is adopted in this study.

Now we consider some modifications to equation (15). The term $\alpha\mathbf{q}^*$ (eventually $\alpha\mathbf{q}^n$ in the iterative process) would lead to an increment $\Delta\mathbf{q}^1$ and a better estimation for the first value of the first heat flux $\mathbf{q}^1$. This term makes the calculation more cumbersome with very little benefit in convergence and, therefore, will be neglected, and the equations may be written as:

$$(\mathbf{X}^{\mathrm{T}}\mathbf{X} + \alpha\mathbf{I})\Delta\mathbf{q}^{1} = \mathbf{X}^{\mathrm{T}}\Delta\mathbf{T}^{*} \tag{18a}$$

$$\mathbf{q}^{1} = \mathbf{q}^{*} + \Delta\mathbf{q}^{1} \tag{18b}$$

$$(\mathbf{X}^{\mathrm{T}}\mathbf{X} + \alpha\mathbf{I})\Delta\mathbf{q}^{n} = \mathbf{X}^{\mathrm{T}}\Delta\mathbf{T}^{n-1} \tag{18c}$$

$$\mathbf{q}^{n+1} = \mathbf{q}^{n} + \Delta\mathbf{q}^{n} \tag{18d}$$

where n is the number of iterations.

Starting with either equation (15) or equation (18a)-(18d), a number of N flux vectors $\mathbf{q}^{i}$ for $i = 1, \ldots N$, corresponding to each time step, can be estimated simultaneously. When N is equal to the whole time step in the measurement, the method may theoretically be used to obtain the whole time history of heat fluxes.

The focus of this study is, however, more on the application of the method than on the method itself. During the water jet cooling process, the temperature at each measurement point will drop sharply within only a few limited time steps. Such a sharp drop means that a large load or heat flux vector would occur during such a small fraction of the time domain. Other measuring points will have the same phenomena but at a different time window. This means that if the whole domain approach is used there will be a large fluctuation in the load vector, and as a result the convergence of the solution may be significantly affected.

Thus, the number of time steps N is normally less than 10. A "computation window" of size N may be used sequentially to determinate the heat fluxes in the span of time considered. To clarify this procedure, an example is illustrated in the following where we use $N = 3$ at the beginning of the analysis (the same if assuming at any time step). In the first sequence, the heat fluxes at the first three steps may be obtained by iteration as:

$$\begin{pmatrix} \mathbf{q}^{1} \\ \mathbf{q}^{2} \\ \mathbf{q}^{3} \end{pmatrix}^{n+1} = \begin{pmatrix} \mathbf{q}^{1} \\ \mathbf{q}^{2} \\ \mathbf{q}^{3} \end{pmatrix}^{n} + \begin{pmatrix} \Delta\mathbf{q}^{1} \\ \Delta\mathbf{q}^{2} \\ \Delta\mathbf{q}^{3} \end{pmatrix}^{n} \tag{19}$$

The subsequent three heat flux vectors $\mathbf{q}^{4}$ to $\mathbf{q}^{6}$ may be estimated if the temperatures $\mathbf{T}^{3}$ are considered as the initial temperature for the next sequence, and the computation window moves three steps; and so on for each subsequent sequence.

The above procedure presents a hybrid approach between a whole domain one and a true sequential one that will be addressed in the following paragraphs. This hybrid method implies that the heat fluxes at the previous iteration at each time step will be used in the next iteration for the corresponding time step; i.e. at the $(n + 1)$th iteration $\mathbf{q}^{1}$ will be used for the first time step, $\mathbf{q}^{2}$ for the second one, and $\mathbf{q}^{3}$ for the third one. There will be no need for function specification.

In this paper, a completely sequential approach with function specification is used. First, the newly calculated $\mathbf{q}^{1}$ is used for all time steps within the computation window after the first iteration; i.e. a constant function specification is used for this computation window. Second, the computation window moves one time step at the next sequence after obtaining a convergent solution in the current sequence. Once again, using the previous example, the first computation window consists of time step 1 to time step 3; and the second one includes time step 2 to time step 4.

In each time step, the iterative procedure is used until the inversely predicted temperature $\mathbf{T}_c$ converges to the measured temperature $\mathbf{T}_m$. The convergence criteria used to define the acceptance of the predicted temperature are based on an error norm defined by:

$$\text{Error}-\text{norm}^n = \|\Delta \mathbf{T}^n\| \tag{20}$$

Two convergence criteria for ending the iteration process at each time step are used:

$$\text{Error}-\text{norm}^n \leq \delta T \tag{21a}$$

or

$$\frac{\left|\text{Error}-\text{norm}^{n+1} - \text{Error}-\text{norm}^n\right|}{\text{Error}-\text{norm}^n} \leq \varepsilon \tag{21b}$$

The values of δT and ε depend on the measurement error level. The rationale behind using absolute criteria is that while the norm at a given previous iteration is already very small, the relative norm criterion is still not satisfied at the last iteration. For example, if we set $\delta T = 0.5$, $\varepsilon = 0.05$, and assume Error-norm$^n = 0.49$ and Error-norm$^{n+1} = 0.46$ (here $n+1$ is the last iteration), then we have:

$$\frac{|0.46 - 0.49|}{0.49} = 0.06 > 0.05$$

Flowchart

Figure 2 shows a simplified flowchart for the IHCP solution procedure. In the procedure, the initial guess $\mathbf{q}^*$ of heat flux $\mathbf{q}$ may be taken as zero or any other value. However, the heat flux $\mathbf{q}^2$ obtained at the previous sequence may be used as the initial

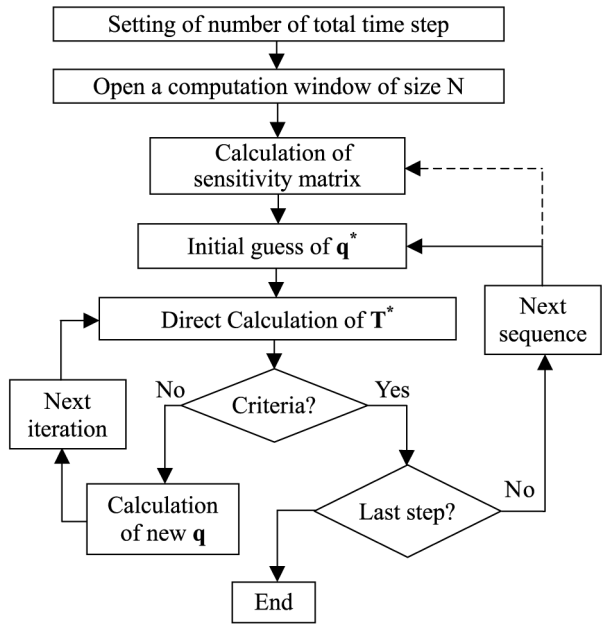

Figure 2.
Flowchart for IHCP solution procedure

guess of heat flux at the current step to accelerate and enhance convergence. The numerical results show that such a setup of the initial guess of the heat flux is better than a random guess.

Parametric studies

Various verification cases have been performed to assess the accuracy, reliability, and stability of the above procedures for both direct and inverse heat transfer calculations. Verification cases for the direct heat transfer analysis were carried out by using both 3- and 6-node triangular elements and 4- and 8-node quadrilateral elements. The results were compatible with the commercial program ANSYS (2002) within less than 0.5 per cent difference in all cases. In the following section, we provide only highlights of the test cases performed for inverse analysis and the results obtained.

The inverse analysis procedures are tested with verification cases that are designed to simulate the cooling of steel strips on run-out tables. Typical values of heat fluxes in these applications are provided as an input for a direct analysis, and the direct results are used to verify the inverse analysis. Two cases (triangular and impulse heat flux inputs) are tested to investigate the effects of number of total (future) time steps on the elimination of damping and lagging behaviour, and to identify the appropriate value of the regularization parameters.

The general 2D FE model used for the inverse analysis is shown in Figure 3. The model is 7 mm high and 20 mm wide. In this parametric study, the same discretization is used in both the direct and inverse analyses. In the formulation of inverse analysis, each component of the heat flux vector $\mathbf{q}^i$ is coupled with one of the measurement points. Normally, the target surface would be discretized with much more elements (nodes) than the number of specified heat flux components, and there will be many elements (nodes) between the target locations. In this study, the top surface is cooled and evenly divided into two subregions, and two components of heat fluxes are applied accordingly. Other surfaces are prescribed as thermally insulated. Four points, two on the surface and two 1 mm beneath the surface points, are selected.The temperatures at the two internal points are used in the inverse analysis to estimate both the heat fluxes and the temperatures of the points on the top surface.

The first stage of the verification involves specifying input heat fluxes and solving a direct heat transfer analysis problem to obtain the corresponding temperature field. The second stage involves an inverse analysis whereas the internal temperatures at the target points (here, two locations) calculated from the first stage are used as virtually-measured ones, called as virtual internal temperature later on. From the virtual internal temperatures, the heat fluxes and surface temperatures are inversly

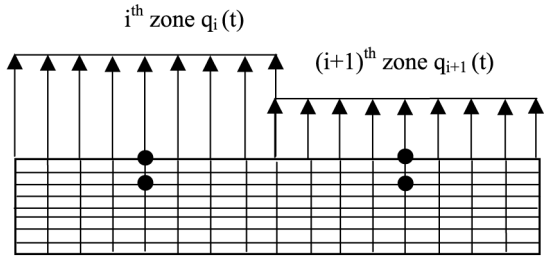

Figure 3.
FE Model for inverse calculation

calculated. A comparison of the inversely calculated surface temperatures to the directly calculated ones is performed to further verify the accuracy and stability of the inverse analysis algorithm.

To study the effects of measurement errors in internal temperatures on inversely calculated heat fluxes, random errors are imposed onto the calculated exact internal temperatures with the following equation:

$$T_{\mathrm{m}} = T_{\mathrm{exact}} + \sigma r \tag{22}$$

where T_{m} is the virtual internal temperature, °C; T_{exact} is obtained from the direct heat transfer analysis, °C; r is a normally distributed random variable with zero mean and unit standard deviation; and σ is the standard deviation, °C. In this work, the maximum additive random error σ is ± 3°C, making a total difference of up to 6°C. In the water jet cooling experiment, the plate temperature ranges from about 900 to 100°C. This means that the relative error has a range of about ± 0.33 per cent (at higher plate temperatures) to ± 3 per cent (at lower temperatures). In the following discussion, we address the error in its absolute value.

The material is assumed to be carbon steel DQSK with a density of 7,800 kg/m^3, a conductivity of 35 W/m°C, and a specific heat of 470 J/kg°Cfor the whole calculation time period. The thermal diffusivity for this steel is about 9.55×10^{-5} m^2/s.

The time step used for both the direct and inverse analyses is the same and is equal to 0.01 s. From the above values, the dimensionless time step is 0.955. This number implies that the inverse calculation may not meet a difficult problem.

The norms for convergence are assigned to be of the order of magnitude of the imbedded measurement error level. The number of future time steps is determined by successive trials and is kept constant throughout the analysis. More discussions about the choice of the regularization parameter will be given in following sections.

Triangular heat flux inputs

Figure 4 shows the two triangular heat flux inputs. They have the same profile and peak value but with a time shift of 0.5 s to produce a spatial temperature gradient in the longitudinal direction.

Inverse analysis is first performed with the assumption that there is no measurement error in the internal temperatures. For this case, the calculated heat

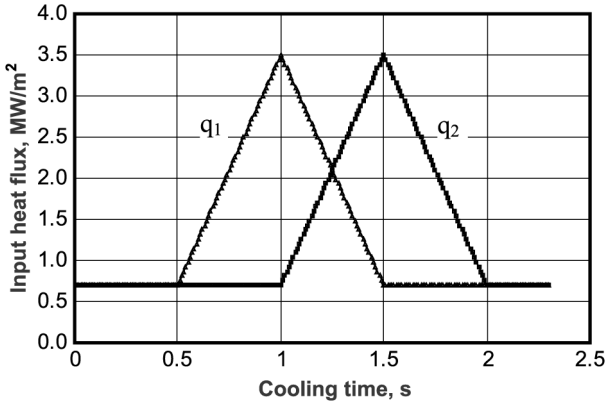

Figure 4.
Triangular heat flux inputs

fluxes match exactly with the input values. The regularization parameter has no effect on the results and may be assumed to be zero, and the number of future time steps also has little effect on the inversely calculated heat fluxes.

Figures 5-7 show the results of those cases studied with various levels of measurement errors and different regularization parameters and future time steps.

Figure 5 shows the effect of the measurement error level on the inversely calculated heat flux with a fixed regularization parameter and a fixed number of future steps. As expected, the heat flux fluctuation increases with the increase of error in the measured temperature. However, the profile of the calculated heat flux is still in good agreement with that of the exact input, and the accuracy of the predicted peak flux value is good.

The effect of the number of future time steps is illustrated in Figure 6. In these cases, the value of the regularization parameter is kept constant at 1.0×10^{-11}, and the error level is fixed at ± 1.0°C. Fewer fluctuations of the calculated heat flux are evident with the increase of the number of future steps. An obvious improvement occurs when the number of future steps increases from 3 to 5, whereas there is slightly less impact for increasing the number of future steps to 5 or 7. It may be concluded that using 4-6 future steps is appropriate and reduces fluctuation levels.

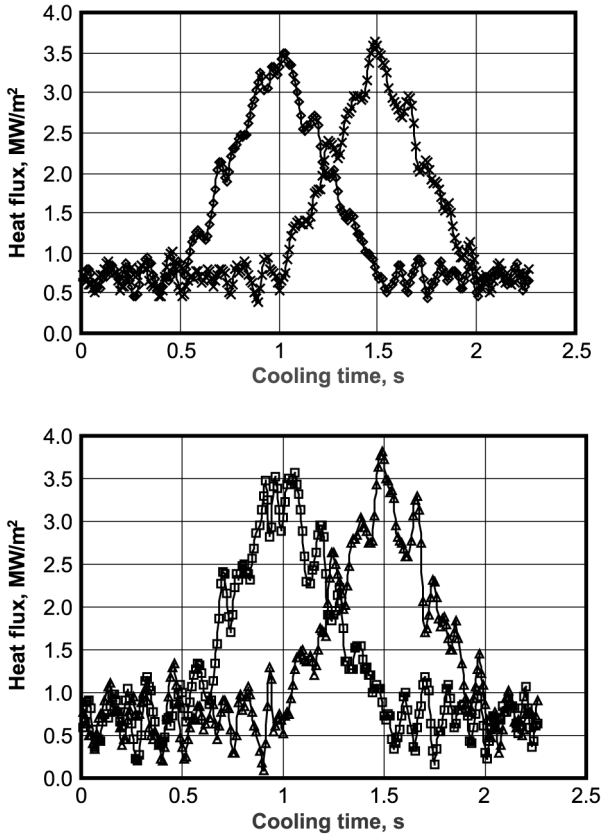

Figure 5.
Effect of measurement error level; $\alpha = 1.0 \times 10^{-11}$; 3 future steps; error level: upper = ± 0.5°C; bottom = ± 1.0°C

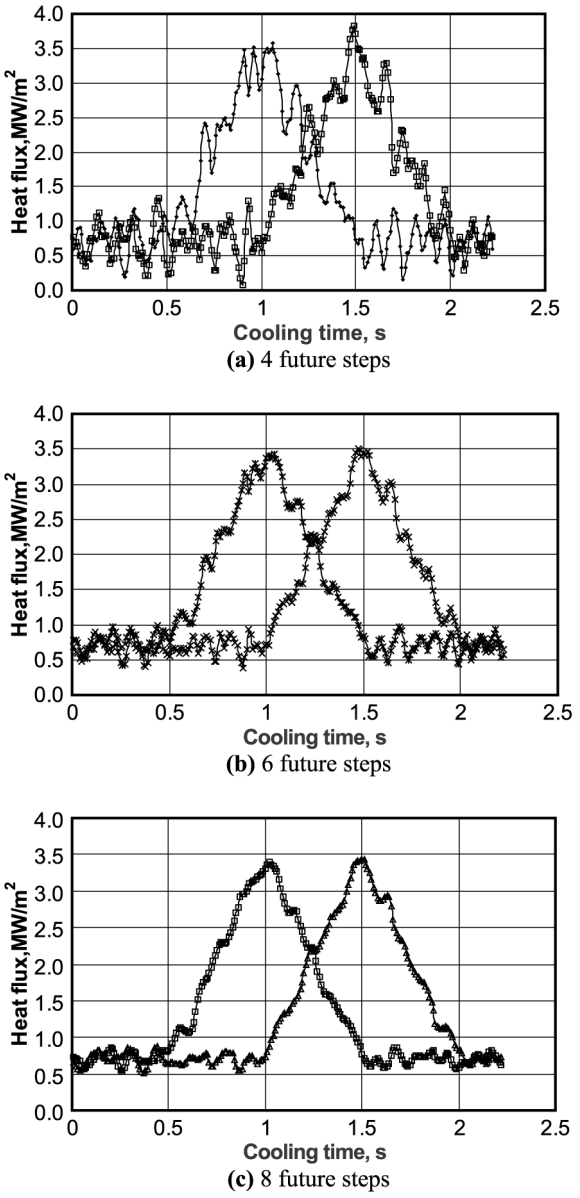

Figure 6.
Effect of number of future steps; $\alpha = 1.0 \times 10^{-11}$; error level = ± 1.0°C

Figure 7 shows the effect of varying the regularization parameter value, α, on the calculated heat flux. Numerical experiments showed that this is a much more delicate parameter to control. Stable and accurate results are obtained for a range of values of $\alpha = 1.0 \times 10^{-10}$ to 1.0×10^{-12}, which is close to the diagonal value of the sensitivity matrix of 1.0×10^{-10}. That is quite an interesting discovery.

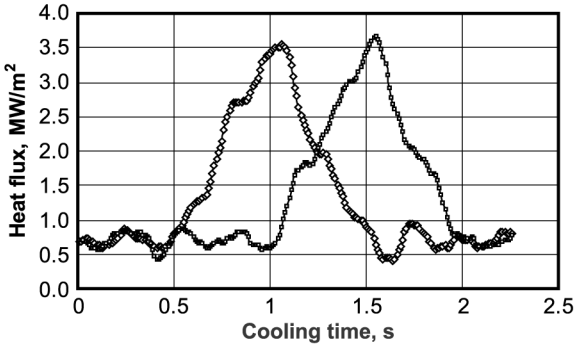

(a) α=1.0e-10

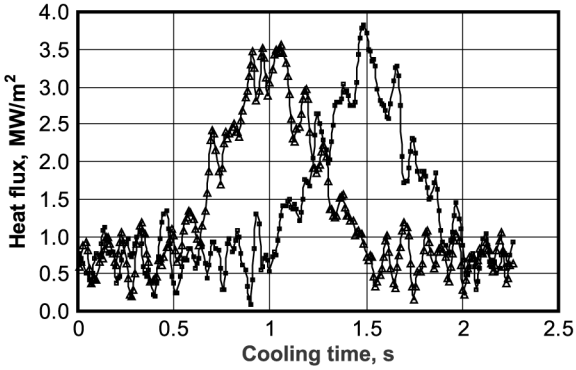

(b) α=1.0e-11

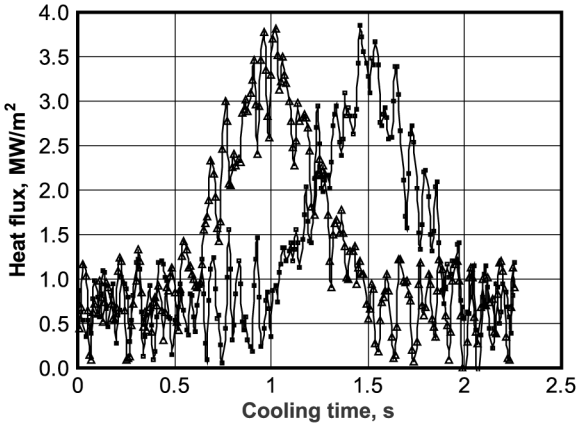

(c) α=1.0e-12

Figure 7.
Effect of regularization parameter; 3 future steps; error level = ±1.0°C

Lowering the value of α to less than 1.0×10^{-14} will increase fluctuations of the inversely calculated heat fluxes, while increasing the value of α to greater than 1.0×10^{-9} greatly increases the required number of iterations and in many cases causes divergence. It should be noted that for all the cases considered above, the maximum difference between the exact value of the surface temperature and the inversely calculated one is only 5°C. This implies that the proposed algorithm might successfully recover both the heat flux and surface temperature.

Impulse-like heat flux inputs

To further examine the capacity of the proposed IHCP scheme and its appropriateness to the simulation of cooling on run-out tables, a second test with impulse-like heat fluxes is performed. The impulse test is known to be the most stringent one for the IHCP algorithms. To simulate the real conditions of a run-out table, a vary high value of heat flux in the order of those experienced practically is applied in a very small time period, equivalent to only five time steps in the solution scheme. The two impulse-like heat flux inputs are shown in Figure 8. The same FE model and procedures discussed in the previous sections are used here.

The inversely calculated heat fluxes under different conditions are shown in Figures 9-11. As in the previous example, the inversely calculated heat fluxes are almost identical to the input ones when no measurement errors are imposed onto the internal temperatures. Also in this case, the regularization parameter has no effect on the inverse results and may be assumed to be zero, and the number of future steps has little effect on the inversely calculated heat fluxes.

Similar to the outcome of the previous example, it is found that with the increase of the measurement errors in the input temperature, the value of both the regularization parameter and the number of future time steps should be increased to obtain acceptable levels of accuracy.

Figure 9 shows a comparison between the calculated heat fluxes using different values of the regularization parameter and a level of ± 1°C error in the measured temperature. Also, the inverse results show that the peak values of heat fluxes are quite

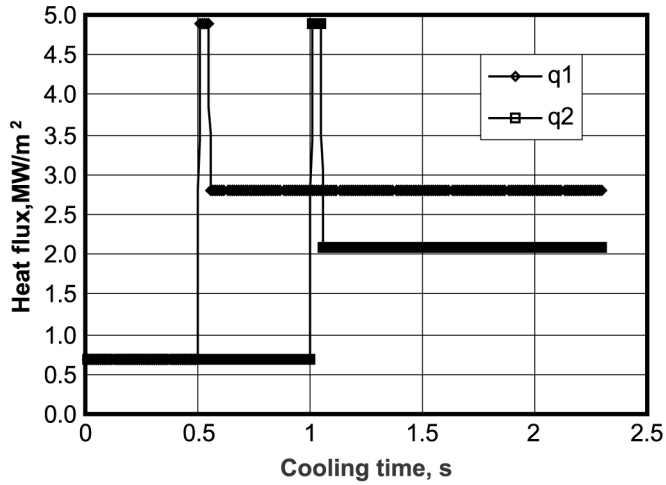

Figure 8.
Impulse-like heat flux inputs

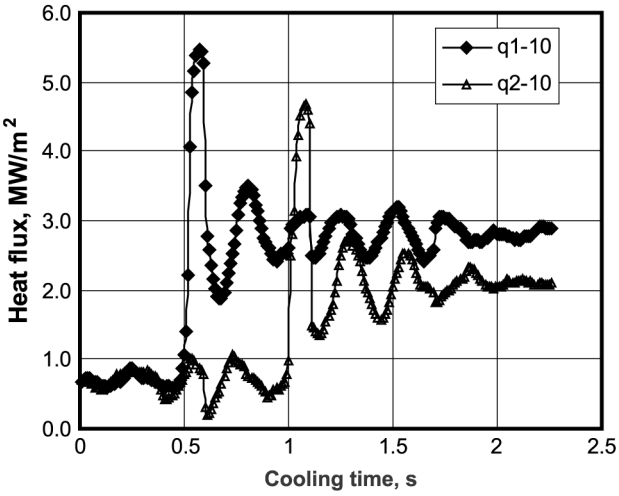

(a) α=1.0e-10 (q1-10, q2-10)

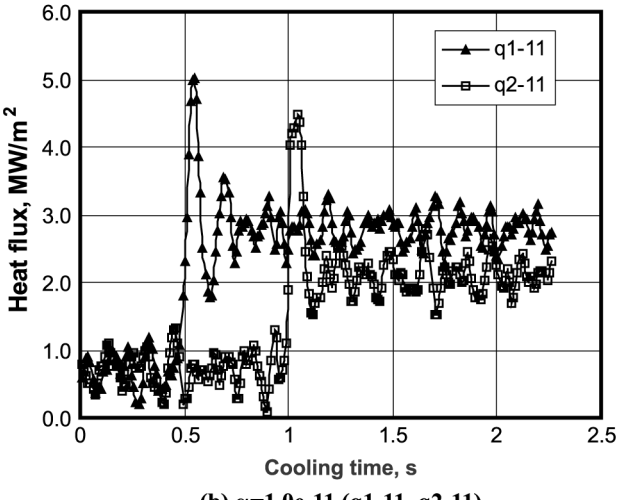

(b) α=1.0e-11 (q1-11, q2-11)

Figure 9.
Effect of regularization parameter; 3 future steps; error level = ±1.0°C

accurate. Even when fluctuations of the calculated values are evident, the average value of the fluctuation represents a good approximation of the exact input. It is also apparent that the regularization parameter has less impact on the fluctuation of the results.

The effect of the number of future steps on the calculated heat flux for the impulse-like heat flux case is shown in Figure 10. It may be seen that there is a somewhat large fluctuation when four future steps are used, and that the fluctuation from the measurement errors is damped gradually with the increase of the number of future steps. When seven future steps are used, the calculated heat flux value is quite close to the input for the period during which the input heat flux is constant.

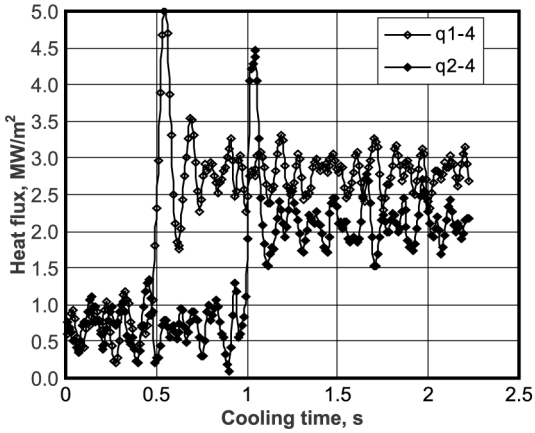

(a) future steps 3 (q1-4, q2-4)

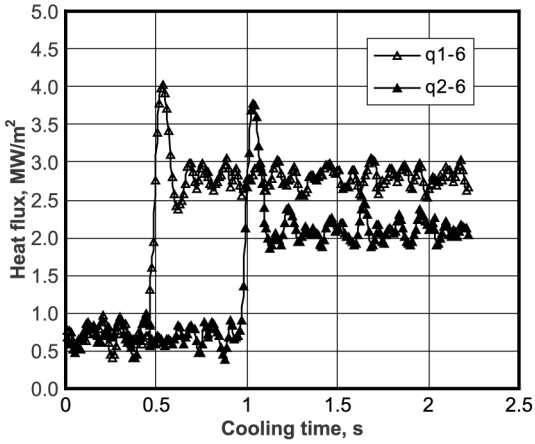

(b) 5 (q1-6, q2-6)

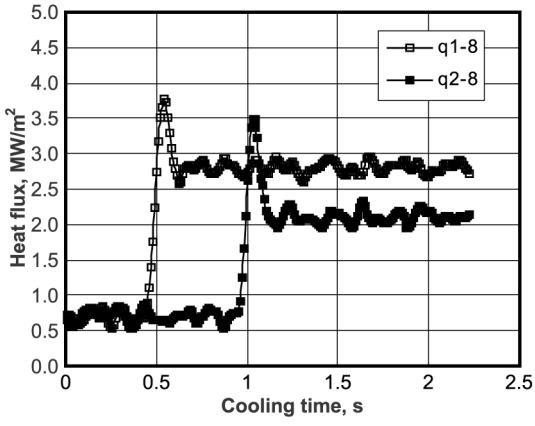

(c) 7 (q1-8, q2-8)

Figure 10.
Effect of future step number; $\alpha = 1.0 \times 10^{-11}$; error level = ± 1.0°C

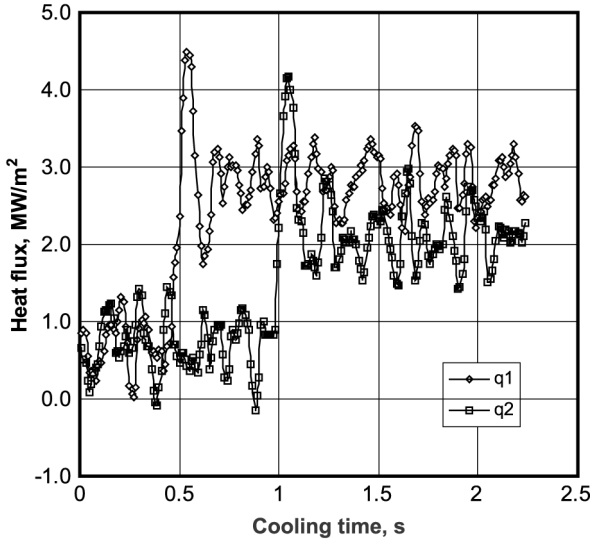

Figure 11.
Calculated heat flux; error level = ±3.0°C; 5 future steps; $\alpha = 1.0 \times 10^{-10}$

However, the peak value is also smeared when the number of future steps increases, although it may still be captured accurately. The damping effect of the future time steps increases significantly when the number of future steps is larger than the number of time steps of the input impulse. This is logical since more weight for the steps with a lower heat flux input is assumed.

With the increase of the measurement error level, both the number of future steps and the value of the regularization parameter should be increased to get reasonable results. Figure 11 shows the calculated heat flux for error level ±3.0°C. The result is obtained by using five future steps and setting $\alpha = 1.0 \times 10^{-10}$

It is obvious that the fluctuation of the estimated heat flux is quite large. Although the peak value seems to be adequately captured, it is difficult to say that this is a real peak because such a peak may come from a larger measurement error. It should be noted that other choices of future time step numbers and regularization parameter do not produce better results. This indicates that the calculated heat fluxes (if a convergence is achieved) would be quite inaccurate if the random error in the actual measured temperature is larger than ±3.0°C.

From the several examples discussed above, we may conclude that the proposed inverse calculation is generally stable and accurate but very sensitive to the measurement error. The calculated peak heat fluxes are in reasonable agreements with the inputs only when the error is not larger than ±3.0°C. It is also apparent that the number of future time steps should be around 3, while the regularization parameter value should be equivalent to the diagonal value of the sensitivity matrix.

Applications

The above procedure is used to investigate heat transfer during the impinging water cooling of steel plates. The intention here is to check the appropriateness of the proposed method for simulating such a complex heat transfer applications.

The experimental setup and procedure are briefly described in this section, and the details can be found in Meng (2002). The test plate dimensions are 280 × 280 × 7 mm.

As shown in Figure 12, thermocouples are installed at eight locations in the circumferential direction on each test plate, starting in the centre of the plate with an increment of 15.9 mm in the radial direction, and they are numbered from 1 in the centre to 8 at the farthest. At each location, an internal thermocouple is installed in a hole with a diameter of 1.6 mm that is drilled from the plate's bottom surface. The measuring junction is fixed onto the end surface of the hole, which is 1 mm below the plate's top surface.

The cooling water impinges from a 19 mm nozzle vertically onto the plate's top surface at the stagnation point where thermocouple T_1 is assumed to be located. Upon reaching the plate surface, water spreads radically outwards.

With the above setup, the problem is assumed to be a 2D axisymmetric one, without considering the effect of the hole used for installing the internal thermocouples.

The material of plate is carbon steel DQSK. Its density and specific heat are assumed to be constant throughout the analysis, with values of 7,800 kg/m^3 and 470 J/kg°C, respectively. The thermal conductivity can be calculated by the following equation with a correlation coefficient of 0.977 and a standard error of 1.0:

$$k = 60.571 - 0.03849 \times T(^{\circ}\mathrm{C}) \ \text{ in } \ \mathrm{W/m^{\circ}C} \tag{23}$$

The above equation is generally valid for a temperature ranging from 0 to 1,000°C.

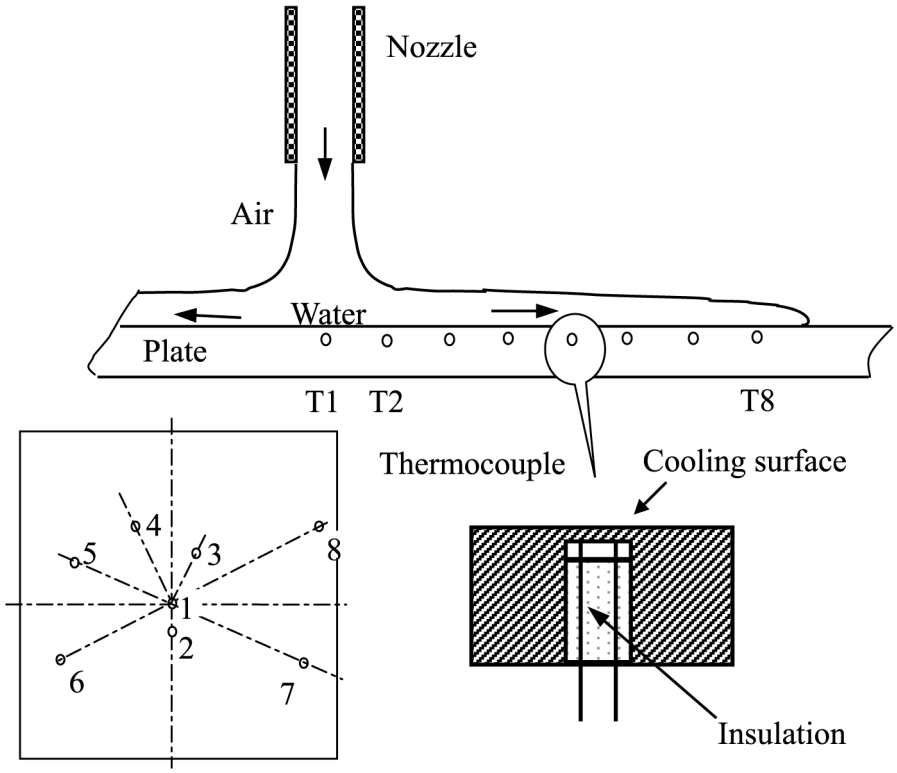

Figure 12.
Schematic arrangements of thermocouples

"Raw" temperatures are recorded at a frequency of 100 Hz. The total recording time of a typical test is about 100 s. The raw data may be directly used in the inverse heat calculation analysis. However, a simple but effective 11-point average smoothing technique is used to filter noise in the internal temperatures. A careful comparison revealed that all the features of the actual cooling curves are retained in the smoothed profiles. In particular, this filtration does not affect the maximum peak of the temperature gradient. It is, therefore, reasonable to expect that the inverse procedure based on the smoothed temperature profile would capture the original characteristic of the heat flux history on the surface. Moreover, the noise in raw temperatures is damped out (the random error is less than ± 3.0°C) and the inverse calculation would probably be more efficient.

Typical cooling curves are shown in Figures 13 and 14. It may be seen that in the air cooling stage the plate temperature is fairly uniform, and it decreases gradually and almost linearly due to radiation and air convection heat transfer. As soon as the water impinges onto the plate the internal temperatures at locations 1 and 2 have an immediate and remarkable drop, and then the gradient decreases slightly, followed by a second sharp drop in temperature. Note that the cooling curves of the temperatures at the first two locations are almost identical for the whole cooling time. From a thermodynamical viewpoint, locations 1 and 2 are within the boundaries of the impingement zone.

With the impingement of cooling water on the plate surface, the temperatures at locations 3-8 begin to decrease. However, the magnitude of the initial drop decreases as the distance from stagnation increases. An important point to note, however, is that

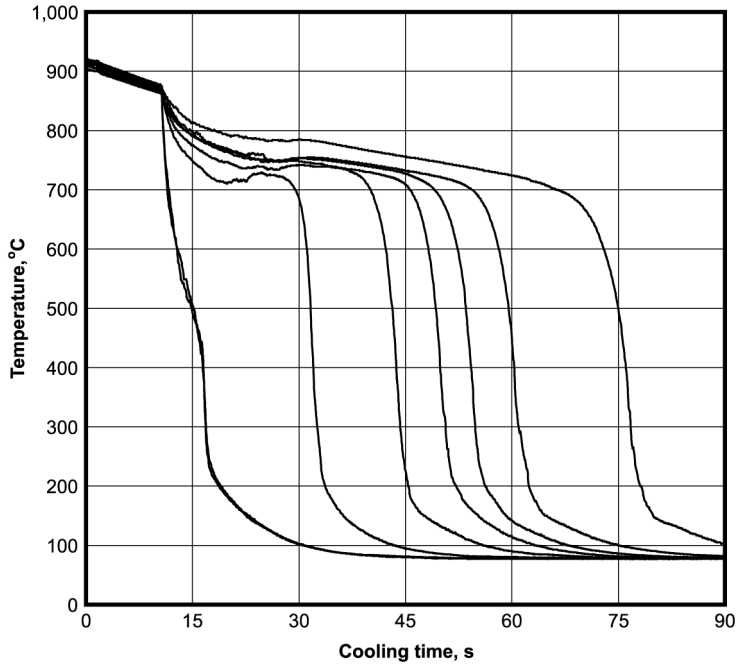

Figure 13.
Example of smoothed measured temperatures; from left to right: T_1 to T_8 (T_1 and T_2 overlapped); DQSK; $\mathbf{Q}_w = 30$ l/min; $T_w = 70$°C; $D_n = 19$ mm

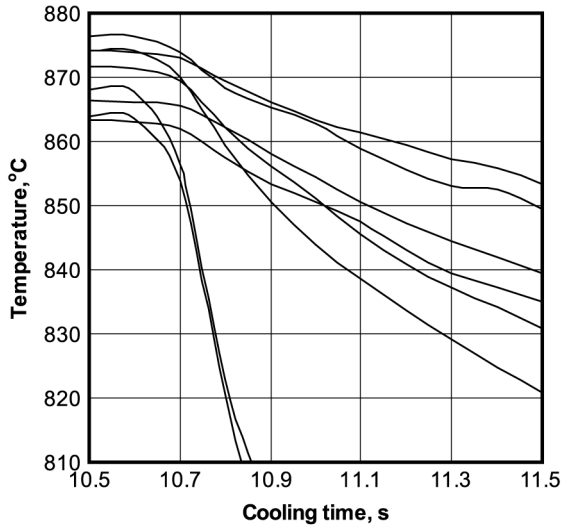

Figure 14.
Part of detailed profile of smoothed temperature

after the initial drop, the temperatures have either a stable and almost flat period or a slight recovery. Following this period, a second significant drop occurs at these locations, and the closer the location from the stagnation point, the earlier the second drop occurs, indicating the arrival of the rewetting front from a thermodynamical point of view. It is worthy to point out that the temperature curves at all locations change their slopes to much smaller values when the temperature reaches about 200°C, suggesting a change of the heat transfer mode.

A full 2D axisymmetric FE model is created for the cooling plate of 115 mm in radius and 7 mm in thickness. There are 2,430 4-node quadrilateral elements and 2,542-nodes in the model. The elements are uniform in the radial direction and vary from fine (on the top surface) to coarse (on the bottom surface) in the thickness direction.

In the inverse calculations, a constant weighted averaged conductivity value of 35 W/m°C (considering that the critical heat transfer happens above 400°C) is used for the whole time span and phase transformation heat is not considered.

The right-hand surface, i.e. the outside of the cylindrical disc, is assumed to be thermally insulated, and a constant heat flux equivalent to air cooling is applied to the bottom surface.

The top surface is divided into eight zones. The first and second zones are equivalent to the impingement zone. The remaining part of the plate is evenly divided into six zones. Each of the eight zones corresponds to one thermocouple. The actual values of heat fluxes at the eight measurement points of temperatures are determined using inverse analysis, and correspondingly applied to the corresponding zone.

In this investigation, the relative norm is fixed at 5 per cent, the absolute norm is 2°C, and the regularization parameter is fixed at 1×10^{-10} (equivalent to the diagonal value of the sensitivity matrix). The number of future time steps changes for different cases.

The full view of heat flux histories, based on the smoothed temperatures corresponding to Figure 13, is shown in Figure 15. In the calculation, only the data at the current time step is used, i.e. no future step is used. Only a few iterations are needed to get a convergent result for each step.

The results in Figure 15 reveal all features of its corresponding temperature curves. For the air cooling stage, the heat fluxes at all locations have relatively close values of about 14 KW/m^2, which is typical due to the combination of radiation and air convection cooling.

As the water hits the plate, the heat fluxes at locations 1 and 2 instantaneously jump to a very high value. After the initial jump corresponding to the initial drop of temperature, there is another drop of heat flux, and then a second extensive jump occurs. The profile of these two curves is repeated for most of the cooling time. The differences in heat fluxes come from the slight difference in temperatures. The highest value of heat flux is 6.0 and 5.5 MW/m^2 at locations 1 and 2, respectively. These values are in good agreement with the findings in the literature Liu *et al.* (2002).

The heat fluxes at locations 3-8 jump at different instants, inversely proportional to the distance from the stagnation point. The magnitudes of the highest heat fluxes of 0.4-1.0 MW/m^2 are much lower than those at locations 1 and 2. The slight recovery of temperatures in Figure 13 leads to a positive heat flux (negative value in the figure), which in practice may result from the phase transformation heat. When the cooling water gradually rewets the top surface, the heat fluxes at these locations rapidly increase, and then decrease at nearly the same speed. The shapes of heat flux profiles are almost identical. The highest values at those locations are about 3.5-4.3 MW/m^2.

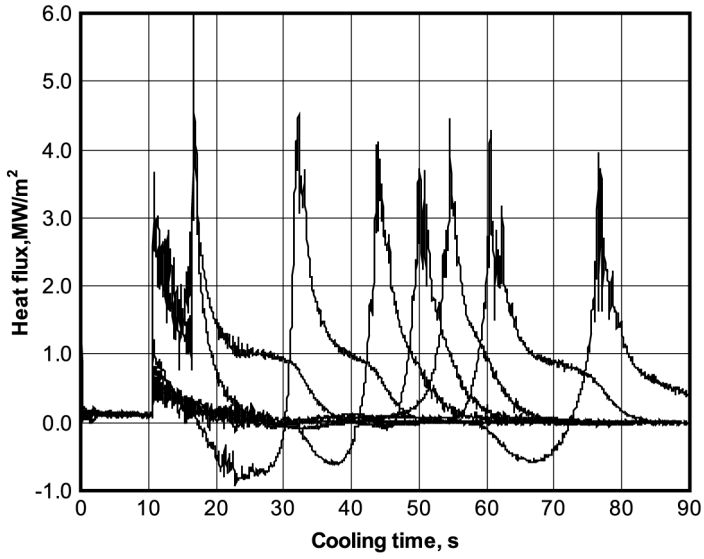

Figure 15.
Full views of heat flux histories on the top surface; from left to right: q1 to q8; DQSK; $Q_w = 30$ l/min; $T_w = 70$°C; $D_n = 19$ mm

The boiling curve is the presentation of heat flux as a function of the wall superheat ΔT_{sat} (the difference between the surface and the saturation temperatures). When the saturation temperature is constant, the relationship between the heat flux and surface temperature may display the characteristic of a boiling curve. Figure 16 shows the boiling curves for the three locations 2, 4, and 6. It is clear from the *P*2 curve for the impingement zone that the transition and nucleate boiling temperature is about 740°C, and that the maximum heat transfer occurs at about 210°C, which is generally in very good agreement with the experimental results (Ishigai *et al.*, 1978). These results are also reasonable from a thermodynamics point of view.

To investigate the detailed heat transfer in the impingement zone, a small model for the impingement area of 21 mm in radius and 7 mm in thickness, which is slightly bigger than the plate portion inscribed by location 2, is considered. 2D axisymmetrical conditions are assumed, and the measured temperatures at locations 1 and 2 are used in this model. Like the full model, the right-hand surface, i.e. the outside of the cylindrical disc, is assumed to be thermally insulated, and a constant heat flux equivalent to air cooling is applied to the bottom surface.

Two cases are studied. In the first case, two different heat flux components are assumed on the plate's top surface (Figure 3) and correspond to the two measured temperature histories. In the second case, only one heat flux component is prescribed on the plate's top surface. The second situation means that the unknowns are less than the temperature measurements, and so we have an overdetermined inverse problem, which would be, generally, more stable. In these two cases, different numbers of future time steps are adopted to investigate the improvement in stability. The results obtained from this model are shown in Figures 17 and 18 where 0F and 3F indicate the heat flux with 0 and 3 future steps.

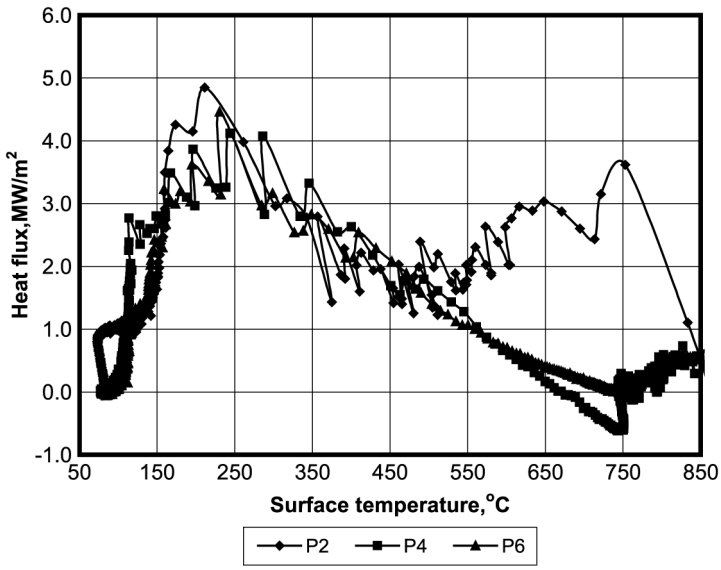

Figure 16.
Boiling curves; DQSK;
$\mathbf{Q}_w = 30$ l/min;
$T_w = 70$°C; $D_n = 19$ mm

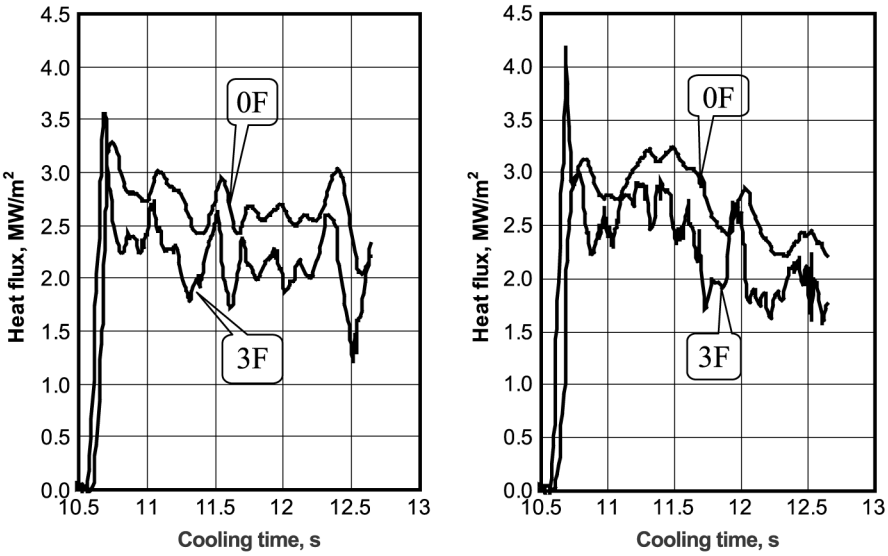

(a) Component 1 **(b)** Component 2

Figure 17.
Heat flux in water impingement zone; two components of heat flux assumed; DQSK; $\mathbf{Q}_w = 30$ l/min; $T_w = 70$°C; $D_n = 19$ mm

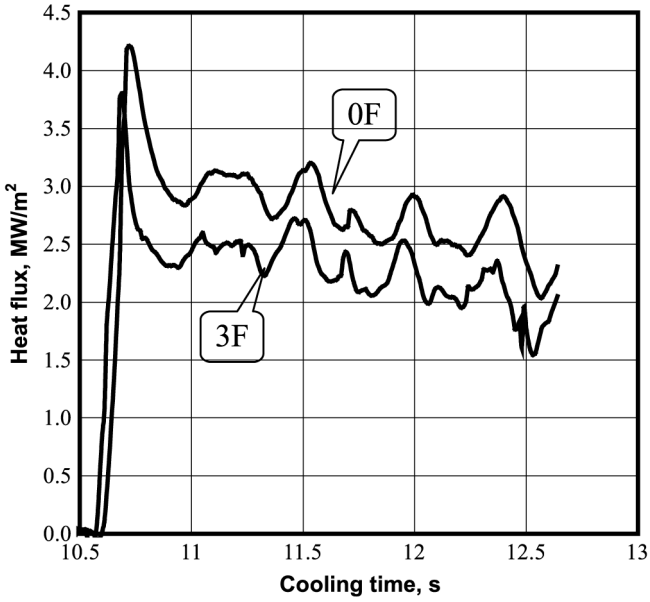

Figure 18.
Heat flux in water impingement zone; one component of heat flux assumed; DQSK; $\mathbf{Q}_w = 30$ l/min; $T_w = 70$°C; $D_n = 19$ mm

Figure 17 is for the case whereas assumption of two heat fluxes is used, and shows the effects of the number of future steps on the inversely calculated heat fluxes in the impingement zone for the instant of impingement and shortly thereafter. There is a sharp jump in the heat flux values at the instant of impingement, followed by a much smaller but sharp decrease to a value that steadily decreases at a slow rate. Calculations verified that there is little difference between the results for the numbers of future steps larger than 3. This indicates that similar cooling conditions exist for a smaller area in the centre of the jet that may be considered as a single cooling zone, the impingement zone.

This conclusion may be confirmed by comparing the results in Figure 18, using the assumption of one component of heat flux on the top surface, to those in Figure 17. The insensitivity of these results to the number of future steps may indicate that the random error in internal temperature measurement is filtered out due to the average smoothing technique discussed above.

Comparison of Figure 15 with Figures 17 and 18 leads to the conclusion that the simplified model may be efficiently used to study the heat transfer behaviour in the impingement zone, which has a diameter approximately equal to twice the diameter of the nozzle for this test condition.

Figure 19 shows the heat flux history at the second thermocouple location for a longer cooling time. The figure shows an initial sharp increase in heat flux value to about 3.7 MW/m^2 as soon as water impinges onto the plate's surface, and then a decrease to a value of 2.1 MW/m^2, which remains as an average value during this period of water cooling. The heat flux value of 2.1 MW/m^2 is consistent with those reported in Colas (1994) and Osman (1990). The second sharp increase to about 4.7 MW/m^2 takes place at a temperature of around 400°C, which indicates the Leidenfrost point.

The HTC at the stagnation point is shown in Figure 20. It may be seen that the HTC holds constant regardless of the calculated surface temperature if the surface temperature exceeds 400°C. This trend coincides with the experimental findings reported in Otomo *et al.* (1987).

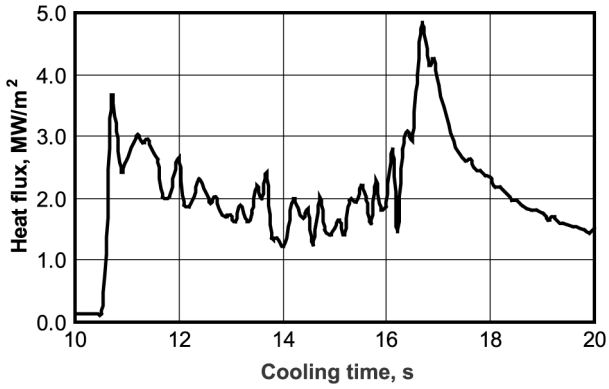

Figure 19.
Heat flux at the second location; DQSK; $\mathbf{Q}_w = 30$ l/min; $T_w = 70$°C; $D_n = 19$ mm

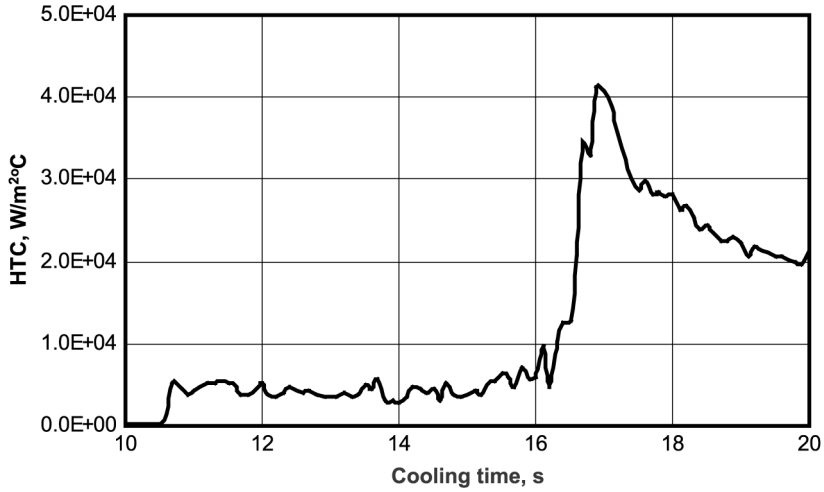

Figure 20.
Heat transfer coefficient at stagnation point; DQSK; $\mathbf{Q}_w = 30$ l/min; $T_w = 70$°C; $D_n = 19$ mm

Summaries

A general 2D FEA program for direct and inverse heat transfer analyses is developed. In the proposed inverse method, the least-squares method, sequential function specification, and regularization are used. And the sensitivity matrix is calculated only once at the beginning of the calculation span, and used for all steps. The iterative technique is adopted to compensate the use of the regularization parameter and the simplification in sensitivity matrix calculation. Two criteria are used for convergence. A parametric study indicates that in inverse calculation the fluctuation of inversely calculated heat flux due to random errors in the measurement data may be damped by increasing the number of future steps and the value of regularization parameter.

Experimental results for the cooling of a stationery hot plate are analysed and assessed using the proposed procedures. The heat flux values and profiles are consistent with those in the literatures. It is also verified that the impingement zone is about two times the diameter of the nozzle for the test conditions presented, and that the simplified model is capable of determining the heat transfer behaviour in the impingement zone.

All calculations show that the presented algorithm and procedures are very simple, useful, and effective in recovering the heat flux history on the cooling surface, and are appropriate for the IHCP in run-out table cooling applications. The proposed procedure is currently being used to study the thermodynamics during the circular jet impingement cooling process of both stationary and moving plates.

References

Alifanov, O.M. (1994), *Inverse Heat Transfer Problem*, Springer, Berlin.

ANSYS (2002), *ANSYS User's Manual*, Swanson Analysis Systems Inc., Houston, PA.

Bass, B.R. (1980), "Application of the finite element method to the nonlinear inverse heat conduction problem using Beck's second method", *Journal of Engineering and Industry, Transaction ASME*, Vol. 102, pp. 168-76.

Bathe, K.J. (1982), *Finite Element Procedures in Engineering Analysis*, Prentice-Hall, Englewood Cliffs, NJ.

Beck, J.V., Blackwell, B. and Clair, C.R.S. Jr (1985), *Inverse Heat Conduction: Ill-posed Problem*, Wiley, New York, NY.

Beck, J.V., Blackwell, B. and Haji-Sheikh, A. (1996), "Comparison of some inverse heat conduction methods using experimental data", *International Journal of Heat and Mass Transfer*, Vol. 39, pp. 3649-57.

Colas, R. (1994), "Modelling run out table cooling", *Manufacturing Science and Engineering American Society of Mechanical Engineers*, Vol. 68, pp. 611-7.

Ishigai, S., Nakanishi, S. and Ochi, T. (1978), "Boiling heat transfer for plane water jet impinging on a hot surface", paper presented at Sixth International Heat Transfer Conference, Toronto, August.

Khache, R.A. and Jarny, Y. (2001), "Determination of heat sources and heat transfer coefficient for two-dimensional heat flow-numerical and experimental study", *International Journal of Heat and Mass Transfer*, Vol. 44, pp. 1309-22.

Kim, H.K. (2001), "Evaluation of heat transfer coefficient during heat treatment by inverse analysis", *Journal of Material Processing Technology*, Vol. 112, pp. 157-65.

Kim, S.K. and Lee, W.I. (2002), "Solution of inverse heat conduction problems using maximum entropy method", *International Journal of Heat and Mass Transfer*, Vol. 45, pp. 381-91.

Liu, Z.D., Fraser, D. and Samarasekera, I.V. (2002), "Experimental study and calculation of boiling heat transfer on steel plates during run-out table operation", *Canadian Metallurgical Quarterly*, Vol. 41, pp. 63-74.

Meng, Q. (2002), "Experimental study of transient cooling of a hot steel plate by an impinging circular jet", Master's thesis, The University of British Columbia, Vancouver.

Osman, A.S. (1990), "Investigation of transient heat transfer coefficients in quenching experiments", *Journal of Heat Transfer, Transaction ASME*, Vol. 112, pp. 843-8.

Otomo, A., Yasungaga, S. and Ishida, R. (1987), "Cooling characteristics of steel sheet by water film in hot strip mill", *Journal of Iron & Steel Institute Japan*, Vol. 73, pp. 996-1003 (in Japanese).

Videcoq, E. and Petit, D. (2001), "Model reduction for the resolution of multidimensional inverse heat conduction problems", *International Journal of Heat and Mass Transfer*, Vol. 44, pp. 1899-911.

Weber, C.F. (1981), "Analysis and solution of the ill-posed inverse heat conduction problem", *International Journal of Heat and Mass Transfer*, Vol. 24, pp. 1783-92.

Appendix. Finite element matrix equations

The governing equation for conduction heat transfer in a 3D solid is given by:

$$\rho c_p \frac{\partial T}{\partial t} = \left[\frac{\partial}{\partial x}\left(k_x \frac{\partial T}{\partial x}\right) + \frac{\partial}{\partial y}\left(k_y \frac{\partial T}{\partial y}\right) + \frac{\partial}{\partial z}\left(k_z \frac{\partial T}{\partial z}\right)\right] + q^b \tag{A1}$$

where k_x, k_y, k_z are the thermal conductivities in x, y and z directions, respectively, T is the temperature, q^b is the internal rate of heat generated per unit volume, t is time, ρ is the density and c_p is the specific heat.

The sources of nonlinearity in equation (A1) may be due to temperature dependent material properties or dependency of the BC on temperature. The above equation may be subject to one or a combination of the following BC:

Prescribed temperature. This is an example of the *Dirichlet* BC. The prescribed temperature T_s may be a function of time and boundary coordinate (spatial function):

$$T = T_s(x, y, t) \text{ on } S_1 \tag{A2}$$

Prescribed heat flux. The specified heat flux (q_s) may be a spatial function or/and a function of time:

$$-\left(k_x \frac{\partial T}{\partial x} + k_y \frac{\partial T}{\partial y}\right) = q_s(x, y, t) \text{ on } S_2 \tag{A3}$$

where q_s is the specified heat flow per unit area (W/m^2). The prescribed heat flux is an example of the Cauchy's or Neumann BC. If q_s is zero, it will represent a natural BC.

Convection heat exchange. When due to contact with a fluid medium, there is a convective heat transfer on part of the body surface, S_4, we have:

$$-\left(k_x \frac{\partial T}{\partial x} + k_y \frac{\partial T}{\partial y}\right) = h(T_s - T_f) \text{ on } S_4 \tag{A4}$$

where h is the convection heat transfer or film coefficient (W/m$^{2\circ}$C), which may be temperature dependent (nonlinear), T_s is the surface temperature (°C) on S_4, and T_f is the fluid temperature (°C), which may be a spatial or/and time function.

Radiation. Assuming a grey body, the BC is given by:

$$-\left(k_x \frac{\partial T}{\partial x} + k_y \frac{\partial T}{\partial y}\right) = \varepsilon\sigma\left[T_{sr}^4 - T_r^4\right] \text{ on } S_5 \tag{A5}$$

where ε is the emissivity of the body's surface, σ is the Stefan-Boltzmann constant (W/m$^{2\circ}$K^4), T_{sr} is the absolute temperature of surface S_5 (°K), and T_r is the known absolute temperature of the external radiative source (°K). The radiation boundary condition may be dealt with as a nonlinear convective boundary condition with an equivalent temperature dependent film coefficient, κ; where:

$$\kappa = \varepsilon\sigma\left(T_{sr}^2 + T_r^2\right)(T_{sr} + T_r) \tag{A6}$$

The above boundary condition equations may be rewritten to the general form of the BCs:

$$k_n \frac{\partial T}{\partial n} = q^s + h(T_f - T_s) + \varepsilon\sigma\left(T_{sr}^4 - T_r^4\right) \tag{A7}$$

where n is the normal to the boundary and the input heat flux is considered only on pertinent surfaces, i.e. surfaces that have specified BC.

Now, we assume an approximation function for the temperature given by:

$$T(\mathbf{x}) = N_i(\mathbf{x})T_i \tag{A8}$$

where $N_i(\mathbf{x})$ is the approximation function with i varying from one to the number of nodes per element, the vector $\mathbf{x}$ has the components x, y and z, and T_i are the nodal temperatures. Note that we consider only a typical element and assume that the normal finite element assembly procedures apply.

Applying the Galerkin approach and using the Gauss theorem, the equivalent finite element equations representing equations (A1) and (A7) may be written in the following final form:

$$[C]\cdot\{\dot{T}^{\mathrm{e}}\}+\left[[K_{\mathrm{c}}]+[K_h]+[K_{\mathrm{r}}]\right]\cdot\{T^{\mathrm{e}}\}=\{Q^{\mathrm{b}}\}+\{Q^{\mathrm{s}}\}+\{Q^h\}+\{Q^{\mathrm{r}}\} \tag{A9}$$

where the definitions of terms in equation (A9) are summarized in Table AI.

Considering the general nonlinear and transient case of equation (A9), the solution may be realized by re-writing the equation at time $(t+\Delta t)$ and ith iteration in the following form:

$$\begin{aligned}&{}^{t+\Delta t}\mathbf{C}^{(i)}t+\Delta t\dot{\mathbf{T}}^{(i)}+{}^{t+\Delta t}(\mathbf{K}^{\mathrm{c}}+\mathbf{K}^h+\mathbf{K}^{\mathrm{r}})^{(i)}t+\Delta t\mathbf{T}^{(i)}\\&=({}^{t+\Delta t}\mathbf{Q}^{\mathrm{b}}+{}^{t+\Delta t}\mathbf{Q}^{\mathrm{s}}+{}^{t+\Delta t}\mathbf{Q}^h+{}^{t+\Delta t}\mathbf{Q}^{\mathrm{r}})^{(i)}\end{aligned} \tag{A10}$$

It may be shown that using the Newton-Raphson approximation and the α-method, the solution to the above equation yields:

$$\begin{aligned}&{}^{t+\alpha\Delta t}\left[(\mathbf{K}^{\mathrm{c}}+\mathbf{K}^h+\mathbf{K}^{\mathrm{r}})+\left(\frac{1}{\alpha\Delta t}\right)\cdot\mathbf{C}\right]^{(i-1)}\Delta\mathbf{T}^{(i)}\\&={}^{t+\alpha\Delta t}(\mathbf{Q}^{\mathrm{b}}+\mathbf{Q}^{\mathrm{s}})+{}^{t+\alpha\Delta t}(\hat{\mathbf{Q}}^h+\hat{\mathbf{Q}}^{\mathrm{r}})^{(i-1)}-{}^{t+\alpha\Delta t}(\hat{\mathbf{Q}}^{\mathrm{c}}+\hat{\mathbf{q}}^{\mathrm{c}})^{(i-1)}\end{aligned} \tag{A11}$$

where the definition of the new terms introduced here are given in Table AII.

$[C]=\int_V\rho c[N]^{\mathrm{T}}[N]\mathrm{d}V$	Thermal capacity matrix
$K_{\mathrm{c}}=\int_V[B]^{\mathrm{T}}[K][B]\mathrm{d}V$	Thermal conductivity matrix
$[K_h]=\int_{\mathrm{S}}h[N^{\mathrm{s}}]^{\mathrm{T}}[N^{\mathrm{s}}]\mathrm{dS}$	Thermal conductivity matrix due to convection BC
$[K_{\mathrm{r}}]=\int_{\mathrm{S}}\kappa[N^{\mathrm{s}}]^{\mathrm{T}}[N^{\mathrm{s}}]\mathrm{dS}$	Thermal conductivity matrix due to radiation BC
$\{Q\}^{\mathrm{b}}=\int_V q^{\mathrm{b}}[N]^{\mathrm{T}}\mathrm{d}V$	Heat flux vector due to internal heat generation
$\{Q\}^{\mathrm{s}}=\int_{\mathrm{S}}q^{\mathrm{s}}[N^{\mathrm{s}}]^{\mathrm{T}}\mathrm{dS}$	Heat flux vector due to input surface flux
$\{Q\}^h=\int_{\mathrm{S}}hT_{\mathrm{f}}[N^{\mathrm{s}}]^{\mathrm{T}}\mathrm{dS}$	Heat flux vector due to convection BC
$\{Q\}^{\mathrm{r}}=\int_{\mathrm{S}}\kappa T_{\mathrm{r}}[N^{\mathrm{s}}]^{\mathrm{T}}\mathrm{dS}$	Heat flux vector due to radiation BC
$\{T\},\{\dot{T}\}$	Vector of global nodal temperatures and temperature gradients, respectively
$\kappa=\varepsilon\sigma\left(T_{\mathrm{r}}^2+T_{\mathrm{sr}}^2\right)(T_{\mathrm{r}}+T_{\mathrm{sr}})$	Equivalent heat transfer coefficient due to radiation
$\left\{\frac{\partial T}{\partial\mathbf{x}}\right\}=\frac{\partial}{\partial\mathbf{x}}(N_i\bar{T}_i)=[B]\{\bar{T}\}^e$	Partial derivative of temperature
$[K]=\begin{bmatrix}k_x & 0 & 0\\ & k_y & 0\\ \mathrm{sym} & & k_z\end{bmatrix}$	Element conductivity matrix
$[N]=\begin{bmatrix}N_1 & N_2 & \cdots & N_n\end{bmatrix}$	Approximation or shape function, n is the number of nodes per element

Table AI.
Definition of the terms in the FE general heat conduction equation

Term	Name	Expression
${}^{t+\Delta t}\hat{\mathbf{Q}}^{h^{(i-1)}}$	Nodal heat flux contribution due to convection BC, nonlinear and transient effects	${}^{t+\Delta t}\hat{\mathbf{Q}}^{h^{(i-1)}} = \int_{S_h}^{t+\Delta t} h^{(i-1)}\mathbf{N}^{S^T}\mathbf{N}^S\left({}^{t+\Delta t}\mathbf{T}_f - {}^{t+\Delta t}\mathbf{T}^{(i-1)}\right)\cdot dS$ Note: $\int_{S_h}^{t+\Delta t} h^{(i-1)}\mathbf{N}^{S^T}\mathbf{N}^S\cdot dS = {}^{t+\Delta t}\mathbf{K}^{h^{(i-1)}}$
${}^{t+\Delta t}\hat{\mathbf{Q}}^{r^{(i-1)}}$	Nodal heat flux contribution due to radiation BC, nonlinear and transient effects	${}^{t+\Delta t}\hat{\mathbf{Q}}^{r^{(i-1)}} = \int_{S_h}^{t+\Delta t} \kappa^{(i-1)}\mathbf{N}^{S^T}\mathbf{N}^S\left({}^{t+\Delta t}\mathbf{T}_r - {}^{t+\Delta t}\mathbf{T}^{(i-1)}\right)\cdot dS$ Note: $\int_{S_h}^{t+\Delta t} \kappa^{(i-1)}\mathbf{N}^{S^T}\mathbf{N}^S\cdot dS = {}^{t+\Delta t}\mathbf{K}^{r^{(i-1)}}$
${}^{t+\Delta t}\hat{\mathbf{Q}}^{c^{(i-1)}}$	Nodal heat flux contribution due to conductivity, nonlinear and transient effects	${}^{t+\Delta t}\hat{\mathbf{Q}}^{c^{(i-1)}} = \int_V \mathbf{B}^T t + \Delta t\mathbf{K}^{(i-1)}\mathbf{B}^{t+\Delta t}\mathbf{T}^{(i-1)}\cdot dV$ Note: $\int_V \mathbf{B}^T t + \Delta t\mathbf{K}^{(i-1)}\mathbf{B}\,dV = {}^{t+\Delta t}\mathbf{K}^{c^{(i-1)}}$
${}^{t+\Delta t}\hat{\mathbf{q}}^{c^{(i-1)}}$	Nodal heat flux contribution due to thermal capacity, nonlinear and transient effects	${}^{t+\Delta t}\hat{\mathbf{q}}^{c^{(i-1)}} = \int_V^{t+\Delta t}(\rho c)^{(i-1)}\mathbf{N}^T\mathbf{N}\cdot\left[\left({}^{t+\Delta t}\mathbf{T}^{(i-1)} - {}^{t}\mathbf{T}\right)/\Delta t\right]\cdot dV$ $\equiv {}^{t+\Delta t}\mathbf{C}^{(i-1)}\left[{}^{t+\Delta t}\mathbf{T}^{(i-1)} - {}^{t}\mathbf{T}\right]/\Delta t$

Table AII.
Definition of the terms in heat transfer equation

Corresponding author
Mohamed S. Gadala can be contacted at: gadala@mech.ubc.ca